Supporting Information

Characterization of Tensioned PDMS Membranes for Imaging Cytometry on Microraft Arrays

Matthew DiSalvo[1], Daniel M. Harris[2, †], Saurin Kantesaria[1], Alexis N. Peña[3], Jules D. Allbritton-King[1], Jacqueline H. Cole[1], Nancy L. Allbritton[1, 3, *]

[1] Joint Department of Biomedical Engineering, University of North Carolina at Chapel Hill, NC 27599, USA and North Carolina State University, Raleigh, NC 27607, USA

[2] Department of Mathematics, University of North Carolina at Chapel Hill, NC 27599, USA

[3] Department of Chemistry, University of North Carolina at Chapel Hill, NC 27599, USA

*Correspondence to: Nancy L. Allbritton, Email: nlallbri@unc.edu.

Joint Department of Biomedical Engineering, University of North Carolina, Chapel Hill, North Carolina 27599, USA and North Carolina State University, Raleigh, North Carolina 27695, USA.
Tel.: +1-919-966-2291; fax: +1-919-962-2388

[†] Current address: School of Engineering, Brown University, Providence, RI 02912, USA

CONTENTS

The supporting information includes the mathematical theory for modeling the deformation of microraft arrays. Also included are discussions of modeling parameters, modeling uncertainty, modeling limitations, the density of data required for accurate modeling, and the effectiveness of alternate shape models. The supplemental methods describe the tensile testing of PDMS, cell culture, and cell staining.

SUPPLEMENTAL EXPERIMENTAL SECTION

Tensile testing. Tensiometry of bulk PDMS was performed according to ASTM D 412 – 06a standards, with the exception of the shape of the dogbone samples, which was rectilinear. The dogbone shape consisted of an 8 mm long, 2 mm wide strip with 10 mm long, 12 mm wide gripping regions at either end. Bulk 3 mm PDMS was die-cut into dogbones and loaded into an EnduraTEC ELF 3200 load frame (Bose). PDMS dogbones underwent 20% strain at 1% s^{-1} rate without pre-loading. The Young's modulus was calculated from the linear slope of the engineering stress as a function of strain. All Young's modulus measurements were taken at room temperature using at least 9 measurements per condition, which included between 2-4 technical and 2-3 experimental replicates.

Cell Culture and Staining. Microraft arrays were prepared for cell culture by air plasma treatment for 5 minutes and sterilization with 75% ethanol. H1299 non-small cell lung carcinoma cells previously transfected with eGFP (H1299-GFP) were seeded on microraft arrays at approximately 2,000 cells/cm^2 and cultured for 5 days in 1:1 fresh:conditioned RPMI media with 10% fetal bovine serum and 1% penicillin/streptomycin until the cells reached a density of approximately 5-10 per microraft. Chemical fixation was performed by rinsing the arrays twice with 1× PBS and incubating them with 1 mL 4% paraformaldehyde at room temperature for 20 minutes. The arrays with fixed cells were rinsed three times with 1× PBS, incubated with 1:250 Hoechst 33342 at room temperature for 15 minutes, and then rinsed three times with PBS. Arrays with fixed and stained cells were stored and imaged in 1× PBS with 0.1% sodium azide.

SUPPLEMENTAL RESULTS AND DISCUSSION

Mathematical model of deflection in transferred microarrays. The transverse deflection of membranes, plates, and shells has been well studied.[1,2] Governing equations and solutions are known for both steady state and non-steady-state deflection phenomena with a variety of model geometries, loading types, and boundary conditions.[3] For thin membranes undergoing small strains, three potential physical bending regimes have been described extensively: 1) no pre-tension, with deformation consistent with plate theory, 2) large pre-tension, with deformation consistent with linear membrane theory, or 3) negligible pre-tension, with deformation consistent with nonlinear solutions.[1] In the case of microraft arrays, pre-tension in the membrane is the dominant component of transverse bending resistance. The deflection of microraft arrays is resisted by both a material bending resistance and resistance due to thermally-induced mechanical tension within the membrane. From plate bending theory, small deflection of thin rectangular plates can be generally modeled by combining the Germain-Lagrange and 2D Poisson equations. The transverse displacement $Z_m(x, y)$ of the membrane under tension T with flexural rigidity D subject to a constant downward pressure with magnitude P thus satisfies the partial differential equation

$$T\left(\frac{\partial^2 Z_m}{\partial x^2} + \frac{\partial^2 Z_m}{\partial y^2}\right) + D\left(\frac{\partial^4 Z_m}{\partial x^4} + \frac{\partial^4 Z_m}{\partial y^2 \partial y^2} + \frac{\partial^4 Z_m}{\partial y^4}\right) = -P. \quad (S1)$$

Assuming that the material parameters are independent of temperature for our experiments, the membrane tension term can be estimated using the relationship

$$T = \frac{Eh\alpha\Delta}{1-\nu}. \quad (S2)$$

where Δ is the difference between the membrane cure temperature and its temperature during deformation measurements, E is the elastic modulus of PDMS, and ν is Poisson's ratio of PDMS.

h is the geometrically averaged thickness of the PDMS membrane, which for square microwells of side length *s*, depth *d* into the membrane of thickness *t*, and distance between adjacent microwells *w* is given by:

$$h = \frac{(t-d)(s)^2 + t((s+w)^2 - (s)^2)}{(s+w)^2}. \quad (S3)$$

The flexural rigidity term is given by

$$D = \frac{Eh^3}{12(1-\nu^2)}. \quad (S4)$$

Mathematically, tension dominates flexural rigidity when $\frac{TL^2}{D} \gg 1$, where the nondimensionalizing factor *L* is the width of the array. Substituting for *D* and *T*,

$$\frac{TL^2}{D} = \frac{12\alpha\Delta(1+\nu)L^2}{h^2} \propto \left(\frac{L}{h}\right)^2. \quad (S5)$$

Microraft array membranes are very thin relative to their width ($\frac{L}{h} \approx 80, \frac{TL^2}{D} \approx 2300$). Thus, the flexural rigidity of the membrane was neglected and the transverse displacement $Z_m(x,y)$ of the membrane under tension T subject to a constant downward pressure with magnitude *P* thus satisfies the linear partial differential equation

$$T\left(\frac{\partial^2 Z_m}{\partial x^2} + \frac{\partial^2 Z_m}{\partial y^2}\right) = -P, \quad (S6)$$

with homogeneous Dirichlet (no-displacement) boundary conditions at the edges of the square membrane with side length *L*, which are $Z_m(0,y) = Z_m(L,y) = Z_m(x,0) = Z_m(x,L) = 0$. The average hydrostatic loading pressure due to the media of volume V was estimated as

$$P = \frac{\rho g V}{L^2} \quad (S7)$$

where ρ is the density of the loading liquid and g is the acceleration due to gravity. The partial differential equation (S6) with boundary conditions was solved using the standard separation of variables technique resulting in the double Fourier series solution for the displacement field

$$Z_m(x,y) = -\frac{16PL^2}{T\pi^4}\sum_{n\ odd}^{\infty}\sum_{m\ odd}^{\infty}\frac{\sin\left(\frac{n\pi x}{L}\right)\sin\left(\frac{m\pi y}{L}\right)}{mn(m^2+n^2)}\ . \quad (S8)$$

The infinite sums (over the positive odd integers only) converge rapidly and thus only a finite number of terms are needed for high accuracy. The spatial structure of the deflection is dictated solely by the infinite sum, whereas the overall amplitude is determined a multiplicative pre-factor depending on the experimental conditions. Using equation (S8), the maximum displacement is predicted to occur at the center of the membrane:

$$Z_m(0.5L, 0.5L) = W \approx -0.0737\frac{PL^2}{T} = -0.0737\frac{\rho g V(1-\upsilon)}{Eh\alpha\Delta}. \quad (S9)$$

Equations (S8-S9) are expected to be accurate for small deflections of dominantly pre-tensioned PDMS membranes with small and shallow microfeatures relative to the membrane thickness. It should be noted the for thin ($h \leq 300$ μm) microarrays under high load ($V \geq 6$ mL of media), the membrane deformation is greater than the array thickness and the use of linear membrane theory for modeling these arrays may produce significant errors.

Modeling parameters. Since the Poisson's ratio and linear thermal coefficient of expansion (CTE) of Sylgard 184 PDMS have been shown to be relatively constant, a Poisson's ratio of 0.5 and CTE of 265 ppm/°C were used for modeling all microarray membranes [4,5] In contrast, the Young's modulus of PDMS varies with the crosslinker concentration, cure temperature, and.[6–9] PDMS cure extent was controlled experimentally by fully curing the PDMS in all conditions with 40-minute cure times. Tensile load testing was used to measure the Young's modulus of

bulk 10:1 and 5:1 PDMS cured at 95 °C. The measurements of Young's modulus, 1.88 ± 0.21 MPa for 10:1 PDMS and 1.47 ± 0.12 MPa for 5:1 PDMS, agree well with literature reports from similarly cured PDMS.[7,10] Additional measurements of the Young's modulus of 10:1 PDMS cured at 150 °C and 10:1 PDMS cured for 48 hours at 95 °C (2.09 ± 0.11 MPa and 1.91 ± 0.24 MPa respectively) were not statistically different from that of 10:1 PDMS cured for 40 minutes at 95 °C, indicating that the PDMS in this study was fully cured.

Discussion of modeling uncertainty. Uncertainty in the material and geometric parameters of microraft arrays exists due to the nature of the microfabrication methods used to make microraft arrays as well as the measurement methods utilized to probe these parameters. The derived equation predicting the maximal membrane deflection of microraft arrays, $Z_m(0.5L, 0.5L) \approx -0.0737\frac{\rho g V(1-\upsilon)}{Eh\alpha\Delta}$, relies on several uncertain parameters. Some are known with high certainty; values for the loading liquid density ρ, gravitational constant g, PDMS Poisson ratio υ, and PDMS coefficient of thermal expansion α are relatively precise in the literature. Others, such as the measured equivalent membrane thickness h had significant variation. A summary of parameter uncertainty is presented in Supplemental Table 1. An estimated propagation of uncertainty was performed under the assumption of no correlation between parameters and that all parameters are constant except E and h:

$$\sigma_{Z_m} \approx \sqrt{\left|\frac{\partial Z_m}{\partial E}\right| \sigma_E^2 + \left|\frac{\partial Z_m}{\partial h}\right| \sigma_h^2}. \quad (S10)$$

Discussion of inconsistent membrane conditions. Microarrays cured at high temperature or fabricated using PDMS with high crosslinker concentrations were poorly predicted by the model (Supp. Fig. 2). Liquid Sylgard 184 PDMS sets (defined by 67% gelation) exponentially faster

with increasing temperature, with previous reports indicating that similar PDMS membranes cured at 130 °C or lower when cured within a 150 °C environment.[11] Finite-element-modeling could potentially be used to compute effective thermal expansion temperatures. However, at cure temperature of 175 °C or greater, thermal degradation and stress defects in PDMS membranes were observed that may have further reduced the accuracy of the model under these conditions.

The measured tensile modulus of bulk 5:1 PDMS was reproducibly and consistently lower than that of 10:1 PDMS in agreement with literature reports.[6,12–14] Yet, reports of PDMS modulus measured by other methods such as nanoindentation, compression, and buckling that are less sensitive to polymer orientation than tensile tests indicate a higher effective modulus.[15,14] We hypothesize that the strength of thin PDMS membranes lies in in the polymer network strength, and tensile measurements of Young's modulus are not always accurate predictors of holistic polymer network strength. However, given the undefined nature of high-crosslinker PDMS, these microarrays were not modelled further.

Fitting deformation models to membrane shape data. It is possible to determine the focal surface of microraft arrays by autofocusing at every imaging position. However, this tactic becomes unfeasible at magnifications above 4× due to the time required to autofocus with typical autofocus routines and microscopy hardware. With a focusing translation speed of 2 mm/s, stage translation speed of 7 mm/s, and image acquisition speed of 10 s^{-1}, the imaging times required to focus throughout a single 1 sq. inch microraft array at 4×, 10×, and 20× magnification are estimated at 0.4, 2.5, and 9.5 hours, respectively. Over these timescales, the media above the PDMS microarrays evaporates altering the load on the array. Not only does this prevent accurate deformation measurements but also leads to cell toxicity from the increased media osmolarity as

the media evaporates over the prolonged analysis times. Thus a method to pair the transferred microraft arrays with a reduced number of focal measurements would significantly improve experiments demanding higher magnification, timelapse imaging, and/or rapid single-timepoint microscopy of deforming membranes.

A series of parameters were added to the physical model describing membrane deflection in equation (S8) to enable fitting to real-world microarray data. In practice, the precise material and geometric parameters of a given microarray is seldom known exactly. Furthermore, in optical assays, arrays are typically placed with small tilts and focal offsets relative to the measurement coordinate system of microscope stages. A lumped-parameter approach describing the transverse displacement of microraft arrays was adopted to account for unknown material and/or geometric microarray parameters:

$$Z_m^{lumped}(x, y, A) = A \sum_{n\ odd}^{\infty} \sum_{m\ odd}^{\infty} \frac{\sin\left(\frac{n\pi x}{L}\right) \sin\left(\frac{m\pi y}{L}\right)}{mn(m^2 + n^2)}, \quad (S11)$$

where the aggregate parameter A is a linear scale factor. Membrane tilts and offsets relative to the coordinate system of the microscope stage were compensated for by modifying equation (S11) with a uniform planar offset to form the fitting equation

$$Z_m^*(x, y, A, x_0, y_0, z_0, a, b) = Z_m^{lumped}(x - x_0, y - y_0, A) + \left(z_0 + a \times (x - x_0) + b \times (y - y_0)\right), \quad (S12)$$

where fit parameters x_0 and y_0 are the translations in x and y required to center the array and z_0, a, and b are the coefficients of a flat plane that de-trends the membrane onto the X-Y plane of the microscope stage. By considering membranes under no media load as flat planes, measured focal points $Z_m^{measured}(x,y)$ on the membrane of the microarray were fit to equation (S12) in a least-squares manner:

$$\min_{A,x_0,y_0,z_0,a,b} \sum_{x,y} (Z_m^{measured}(x,y) - Z_m^*(x,y,A,x_0,y_0,z_0,a,b))^2. \qquad (S13)$$

The fitting minimization in equation (S13) was implemented as an unconstrained multivariate minimization using MATLAB's *fminsearch* function.[16] Initial guesses of the fit parameters were $x_0 = y_0 = 0$, $z_0 = \max(Z_m^{measured}(x,y))$. Guesses for microraft array tilt angles a and b were produced from a least squares fit of a flat plane to the measured transverse displacement ($Z_m^{measured}$), and the initial guess for the deformation scale (A) was the range of tilt-corrected displacements (Z_m^*). The rapidly converging infinite sum in equation (S11) was implemented using odd m and n from 1 to 25. The search tolerances were 0.001 μm^2 and 0.1 for the function value and fitting parameters, respectively.

A priori information about the microraft array spatial orientation can be incorporated into equation (S13) to improve fitting robustness. The orientation information includes: array focal height on the microscope stage, array tilt angles, and the coordinate of the center of microraft array deformation. When these parameters, symbolized as z_0, a, b, x_0, and y_0, respectively, were treated as constants in equation (S13), the fitting equation was simplified to reducing the fit to a univariate minimization for the array deformation A:

$$\min_{A} \sum_{x,y} (Z_m^{measured}(x,y) - Z_m^*(x,y,A))^2. \qquad (S14)$$

The fitting minimization in equation (S14) was implemented as a bounded minimization using MATLAB's *fminbnd* function.[17]

The measured, unfitted maximal deflection of the microraft arrays was estimated from focal point data as the difference between the highest and lowest point of de-trended measurements of the array surface position. The 95th percentile was used to estimate the highest

and lowest positions in order to minimize the effect of for measurement noise on the estimate of maximal deflection.

Optimization of membrane shape data measurement density. The location and number of deflection measurements that are necessary to obtain an accurate prediction of deflection at all locations of a microarray membrane using equation (S13) were investigated. A training set of microarray shapes was generated by measuring the deformations of four transferred microraft arrays (Condition 1) under 3 and 6 mL liquid load using a 23×14 measurement grid (approximately 0.6 measurements/mm^2). This training set was subsampled from 23×14 down to various measurements resolutions and patterns ranging from 9 to 57 points in size (Supp. Fig. 4). Each subsampled pattern of measurements was fit to a deformation model using equations (S11-S13), and the resulting model was then used to predict the original 23×14 grid of microarray surface positions. The mean absolute difference between the original and interpolated data varied with the number and patterning of measurement points (Supp. Fig. 4A). Averaging over 4 arrays with average maximal deflection of 330 μm, the difference between the original and interpolated reached a minimum of 3.4% with 25 or more measurement points. A measurement pattern of 19 points, or 6% of the original 23×14 grid, was selected as an optimal tradeoff between speed and accuracy (Fig. 4A "Pattern 1").

A disadvantage of the above approach is that the measurement pattern requires focal measurements spanning the entire microarray, and acquiring these measurements becomes more time-inefficient as the arrays scale in size. For the 2.3×2.3 cm microraft arrays in this study, about 13% of the time spent determining a focal surface was used translating the microscope stage between the 19 imaging points, which were on average 6.7 mm away from each other. This

fraction of time would increase to ~40% for a hypothetical 10×10 cm array. Thus, more concentrated patterns of measurements were also of interest (Fig. 4A "Pattern 2" and "Pattern 3").

Rapid determination of microarray imaging surfaces using other shape models. The performance of other shape modeling approaches to enable cytometric microscopy in combination with transferred microrarrays was compared to that of the tension shape model. Thin plate splines, cubic interpolants, and biharmonic interpolants were used to calculate the focal planes for microscopic cytometry of the same array tested by the pre-tension shape model. Of these, only thin plate splines were able to fit data from Patterns 1-3 without massive prediction errors of focal positions outside the 10 mm working distance of the objective. Imaging using thin plate splines to predict focal points from Pattern 1-3 measurements resulted in 2-3 fold more error in cytoplasmic or nuclear area quantification and up to 3 fold more microrafts with errors in cell count greater than 1 cell compared to the tension model (Supp. Fig. 6, Supp. Table 2).

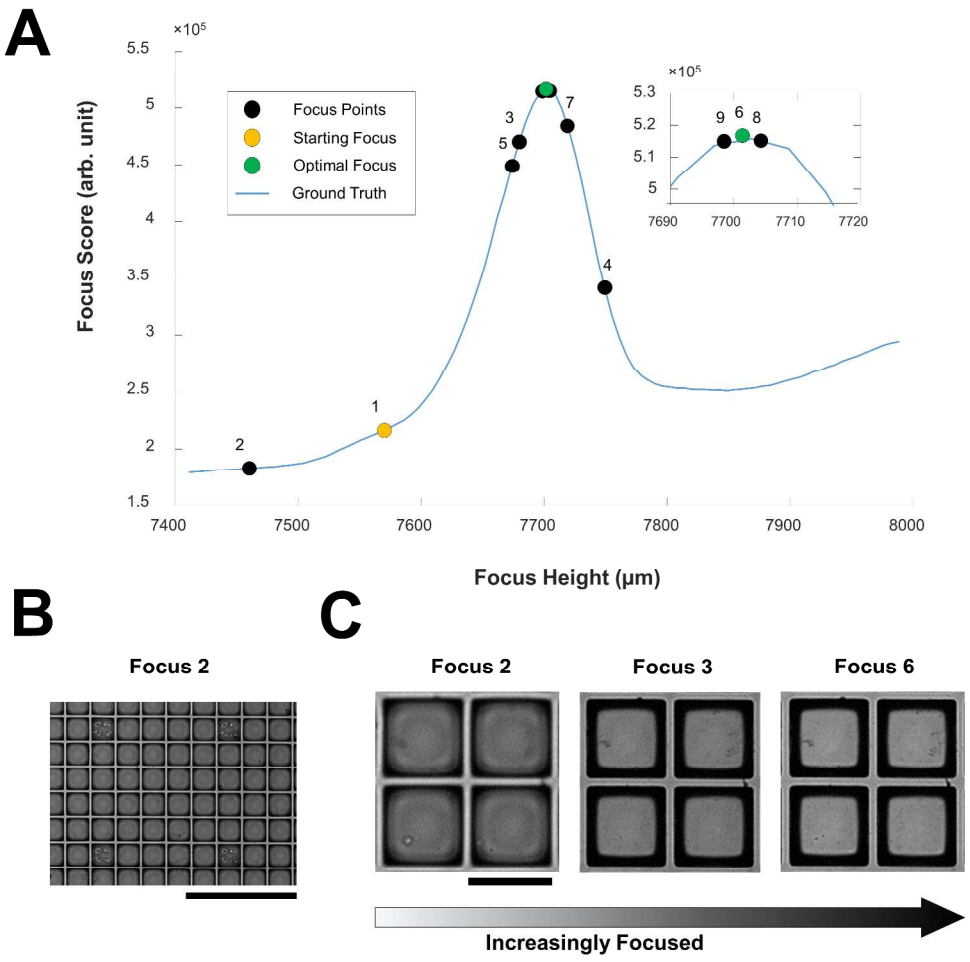
A
×10^5
5.5
5
4.5
4
3.5
3
2.5
2
1.5
Focus Score (arb. unit)
Focus Points
Starting Focus
Optimal Focus
Ground Truth
1
2
3
4
5
7
×10^5
5.3
5.2
5.1
5
9
6
8
7690
7700
7710
7720
7400
7500
7600
7700
7800
7900
8000
Focus Height (μm)
B
Focus 2
C
Focus 2
Focus 3
Focus 6
Increasingly Focused

Supplemental Figure 1. Example focal plane measurements of the microraft array surface used to determine the best focal plane. A microraft array was imaged in an initial plane (plane 1) in bright-field. The grayscale pixel intensity standard deviation ("Focus Score") was measured and then Brent's algorithm was used to determine the next plane for imaging.[17] This process continued iteratively until a maximal focal score was obtained at plane 6 when using a tolerance, or smallest allowable iteration step, of 2 μm. (A) Focal score *vs* the imaged plane is shown for an example autofocus process. The Y axis of 7400-8000 μm is the measured distance from the lowest position available to the microscope objective (0 μm). A high-resolution set of focus measurements taken every 4 microns is included for visualization purposes (blue ground truth trace). (B) A representative bright-field microscopy field of view during focusing. Scale bar is 1 mm. (C) Cropped images at intermediate focal planes as well as the best focus plane showing 4 microrafts. Scale bar is 200 μm.

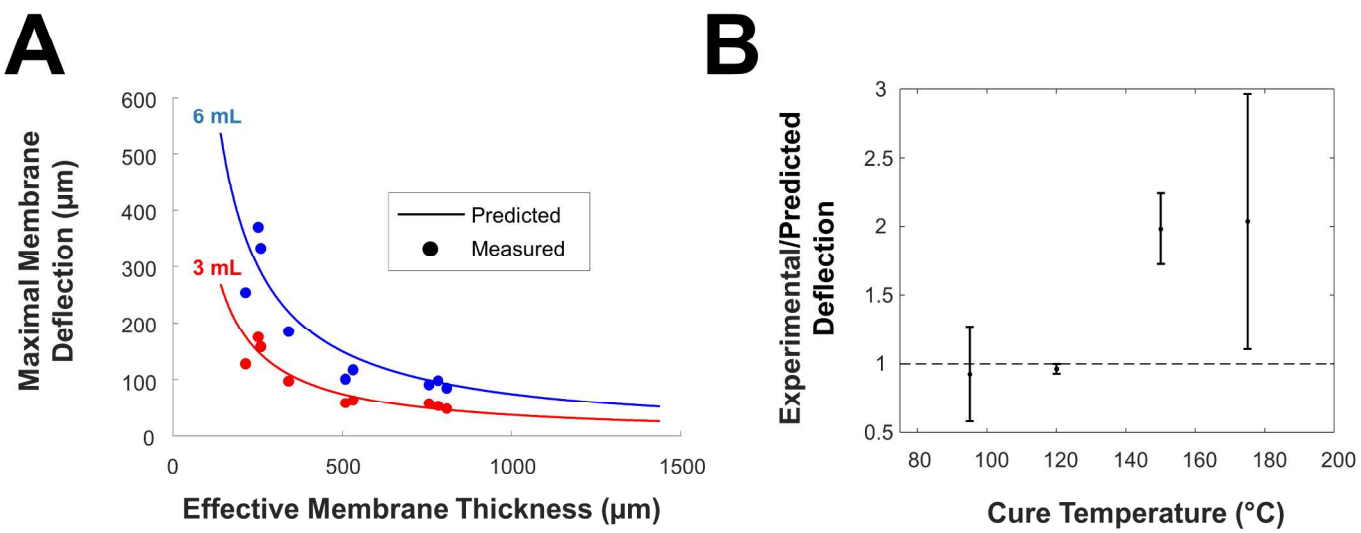

Supplemental Figure 2. Modeling of the microarray deflection at various array thickness and cure temperatures. (A) Fold-difference between experimental and predicted microraft array deflection as a function of PDMS cure temperature for conditions 1-4 and 6-8 of Table 2. The dotted line represents agreement between measured and predicted array deformations. (B) Measured and predicted maximal microarray deflection as a function of PDMS thickness and volume of media placed onto the array for conditions 1, 3, and 4 of Table 2.

Supplemental Table 1. Uncertainty in modeling parameters.

Parameter	Value*	Standard Uncertainty	Relative Standard Uncertainty (%)
E	1.88 MPa	0.21 MPa	11%
h	264 μm	22 μm	8%
Δ	58 °C	2 °C	3%
V	3 mL	0.005 mL	0.2%
α	265 ppm/°C	~	~
v	0.50	~	~
ρ	1000 kg/m^3	~	~
g	9.80665 m/s^2	~	~

*For a representative transferred array (Condition 1, Table 1)

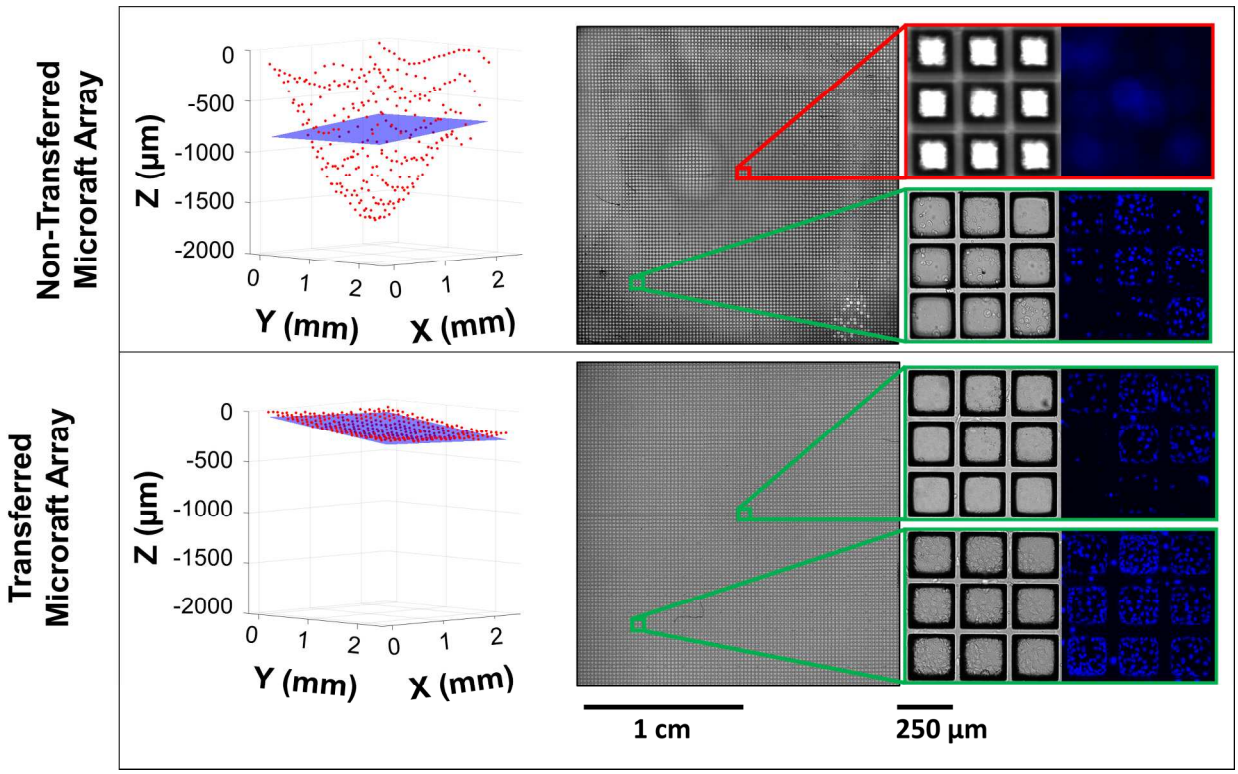

Supplemental Figure 3. Comparison between transferred and non-transferred microraft arrays. (Left panels) Deflection (red) and imaging plane generated from a 1st order polynomial surface fit to the deflection (blue) of microraft arrays. (Middle panel) Widefield view of the microraft array. (Right panels) Bright-field and fluorescence microscopy of H1299 cells adhered to microrafts. Green: Visually judged to be in-focus; red: de-focused; blue: nuclear Hoechst 33342 fluorescence.

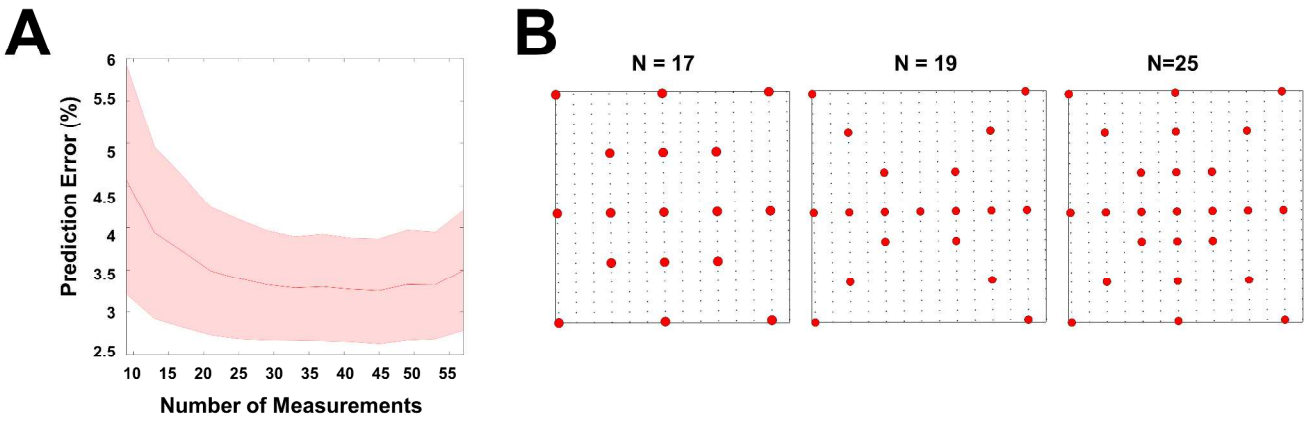

Supplemental Figure 4. Determination of optimal number and pattern of measurements for surface modeling of microraft arrays. (A) The theoretical convergence to minimum error of shape fitting (Y axis) using a variety of patterns and different numbers of measured focal planes (X axis). The mean convergence percent is indicated by the red curve while the shaded error bars represent 1 standard deviation over n=4 datasets. (B) Representative patterns using 17, 19, and 25 measured focal planes are shown. Measurement points are in red, microraft array edges are in black, and the small black points represent all focal plane measurements contained in the datasets from (A).

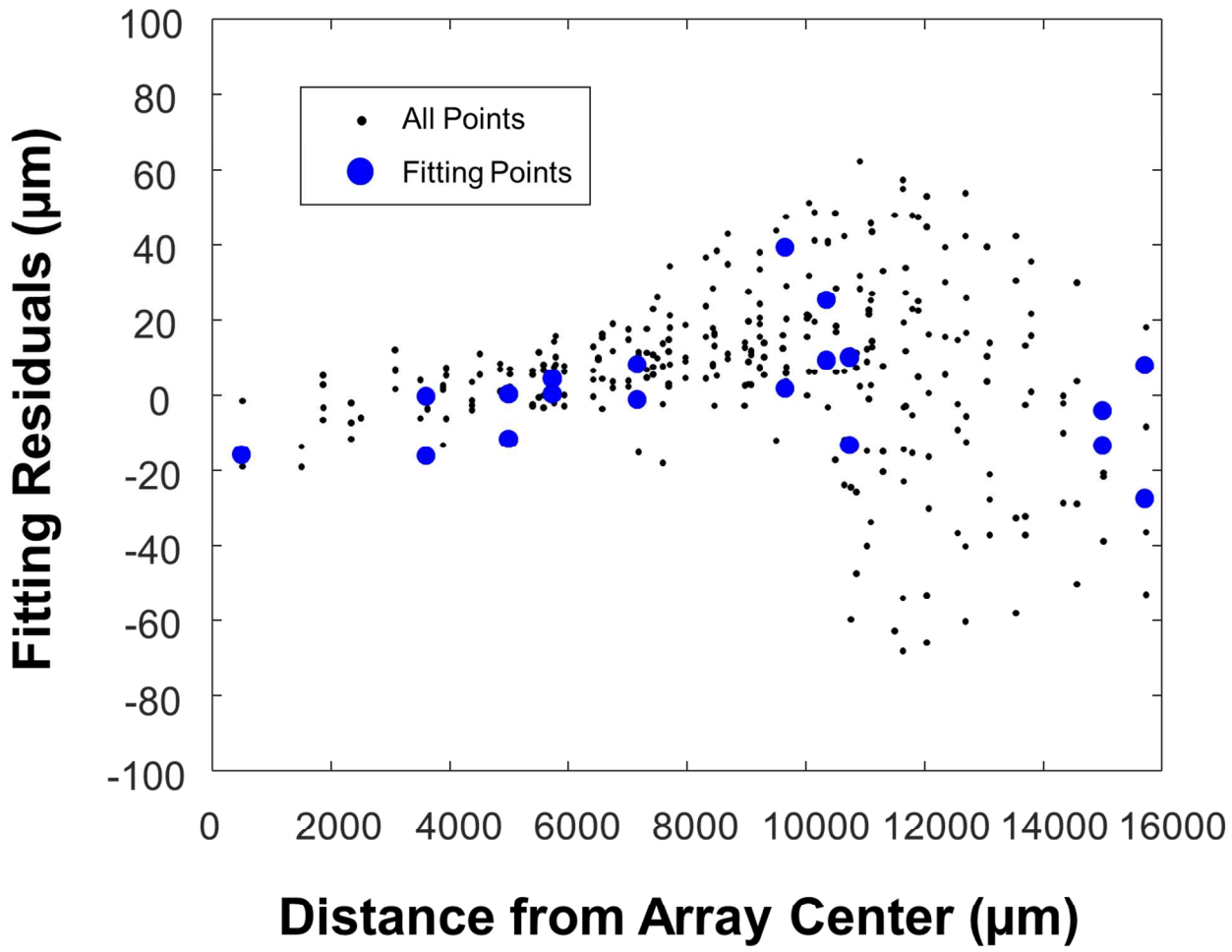

Supplemental Figure 5. Fitting residuals as a function of distance from the microarray center using Pattern 1 focal measurements to predict a 312-point grid of focus locations throughout a microraft array.

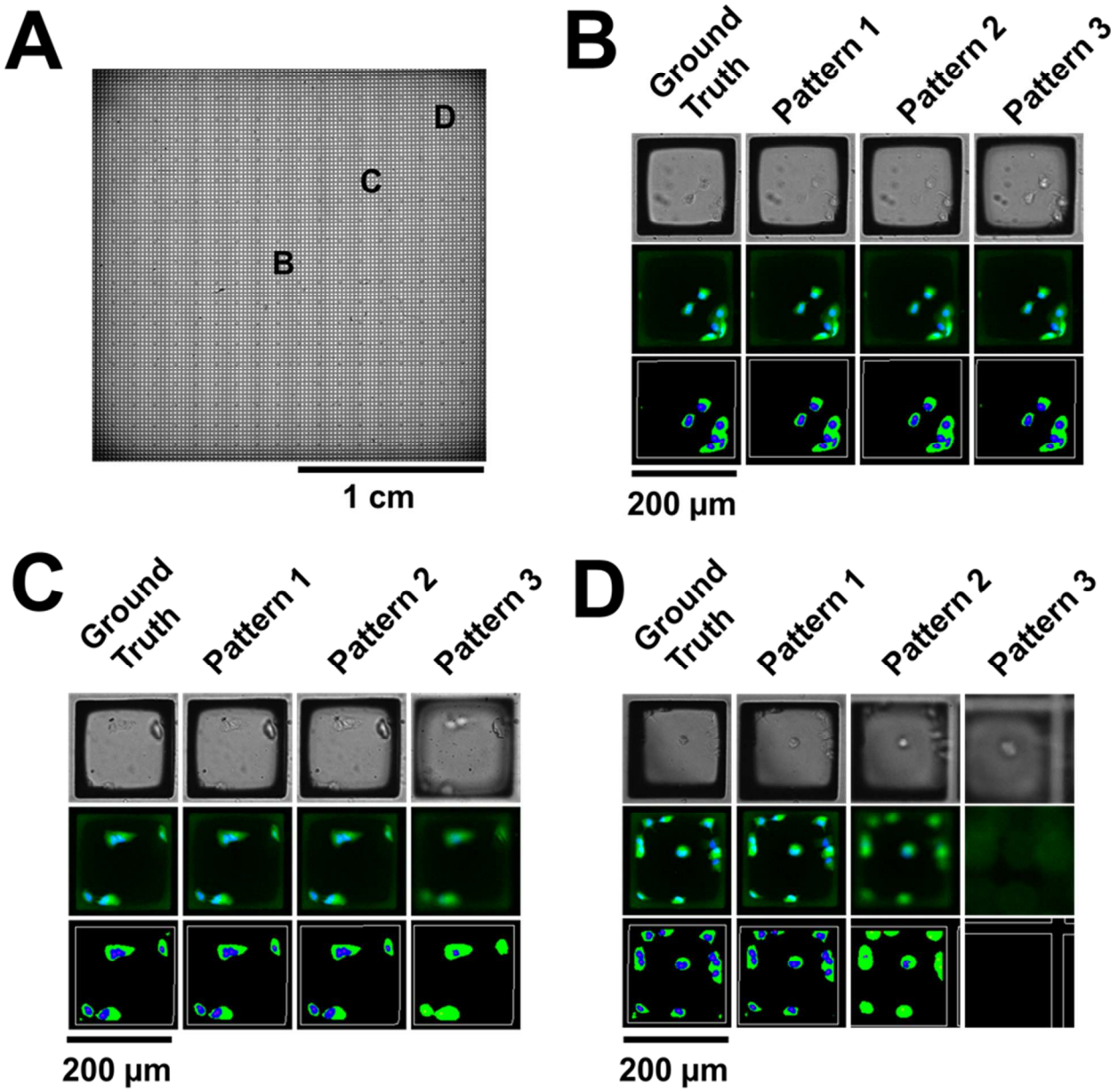
A
D
C
B
1 cm
B
Ground Truth
Pattern 1
Pattern 2
Pattern 3
200 µm
C
Ground Truth
Pattern 1
Pattern 2
Pattern 3
200 µm
D
Ground Truth
Pattern 1
Pattern 2
Pattern 3
200 µm

Supplemental Figure 6. Application of gold-standard thin plate spline model to automated imaging. (A) Whole-array stitched bright-field images of a microraft array seeded with H1299-EGFP cells. (B-D) Images from select regions of the array as indicated in panel A. Close-up bright-field (top row) and composite fluorescence (middle row) images of representative individual microrafts are shown at the three locations. Green: cytoplasmic EGFP fluorescence. Blue: nuclear Hoechst 33342 fluorescence. Also shown are visualizations of identified microrafts (white outline), cell cytoplasm (green) and nuclei (blue) (bottom row) after analysis of the bright-field and fluorescence images.

Supplemental Table 2. Comparison of cytometry performance using thin-plate spline modeling.

Focusing Pattern	Modeling Time (s)	Median Relative Absolute Error (%)				Microraft Analysis Efficiency (%)	Correct Cell Counts (%)	Incorrect* Cell Counts (%)
		Microraft Area	Cytoplasmic Area	Nuclear Area	Cell Count			
Ground Truth	1336.4	0.0	0.0	0.0	0.0	100.0	100.0	0.0
Pattern 1	101.3	0.8	2.7	3.1	0.0	101.5	74.6	18.7
Pattern 2	116.0	1.6	4.4	5.9	0.0	100.2	53.1	25.3
Pattern 3	109.0	1.6	6.8	9.0	12.5	93.5	43.2	24.6

*Error of 1 cell

SUPPLEMENTAL REFERENCES

(1) Komaragiri, U.; Begley, M. R.; Simmonds, J. G. *J. Appl. Mech.* **2005**, *72* (2), 203.
(2) Timoshenko, S.; Woinowsky-Krieger, S. *Theory of plates and shells*; Engineering societies monographs; McGraw-Hill, 1959.
(3) Begley, M. R.; Mackin, T. J. *J. Mech. Phys. Solids* **2004**, *52* (9), 2005–2023.
(4) Lee, T. I.; Kim, M. S.; Kim, T. S. *Polym. Test.* **2016**, *51*, 181–189.
(5) Mark, J. E. Oxford University Press: New York 1999.
(6) Hocheng, H.; Chen, C. M.; Chou, Y. C.; Lin, C. H. *Microsyst. Technol.* **2010**, *16* (3), 423–430.
(7) Johnston, I. D.; McCluskey, D. K.; Tan, C. K. L.; Tracey, M. C. *J. Micromechanics Microengineering* **2014**, *24* (3), 35017.
(8) Khanafer, K.; Duprey, A.; Schlicht, M.; Berguer, R. *Biomed. Microdevices* **2009**, *11* (2), 503–508.
(9) Liu, M.; Sun, J.; Sun, Y.; Bock, C.; Chen, Q. *J. Micromechanics Microengineering* **2009**, *19* (3), 35028.
(10) Schneider, F.; Draheim, J.; Kamberger, R.; Wallrabe, U. *Sensors Actuators A* **2009**, *151*, 95–99.
(11) Wong, E. J. *Ph.D. Thesis* **2010**.
(12) Seghir, R.; Arscott, S. *Sensors Actuators A. Phys.* **2015**, *230*, 33–39.
(13) Seo, J. H.; Sakai, K.; Yui, N. *Acta Biomater.* **2013**, *9* (3), 5493–5501.
(14) Wilder, E. A.; Guo, S.; Lin-Gibson, S.; Fasolka, M. J.; Stafford, C. M. *Macromolecules* **2006**, *39* (12), 4138–4143.
(15) Wang, Z.; Volinsky, A. A.; Gallant, N. D. *Journal of Applied Polymer Science*. 2014.
(16) Lagarias, J. C.; Reeds, J. A.; Wright, M. H.; Wright, P. E. *SIAM J. Optim.* **1998**, *9* (1), 112–147.
(17) Brent, R. P. *Algorithms for minimization without derivatives*; Prentice-Hall: Englewood Cliffs, N.J., 1972.